2018

Comparison Of Sentinel-2 And Landsat 8 OLI In The Mapping Of Soil Salinity In Hyde County, North Carolina

Eleanor Davis
University of South Carolina

Comparison of Sentinel-2 and Landsat 8 OLI in the Mapping of Soil Salinity in Hyde County, North Carolina

by

Eleanor Davis

Bachelor of Arts
The George Washington University, 2016

Submitted in Partial Fulfillment of the Requirements

For the Degree of Master of Science in

Geography

College of Arts and Sciences

University of South Carolina

2018

Accepted by:

Kirstin Dow, Director of Thesis

Cuizhen Wang, Reader

Gregory Carbone, Reader

Cheryl L. Addy, Vice Provost and Dean of the Graduate School

ACKNOWLEDGEMENTS

First and foremost, I would like to acknowledge my advisor, Kirstin Dow, for her endless encouragement, edits, and guidance throughout my thesis process. I would also like to acknowledge my committee members, Cuizhen Wang and Gregory Carbone, for their advice and time as I completed my research. It is because of these three remarkable professors that I have chosen to continue my doctoral research here at the University of South Carolina. In addition, I would like to thank the entire Department of Geography for their support and friendship now and in the future.

Next, I must thank my family. My mother and father, Emily and Anthony, for their support throughout my years of schooling. It is because of them that I first became interested in studying the environment and they have often served as idea sounding boards, paper editors, and patient counselors. My brother, Christopher, is an inspiration to me as he pursues his own geographical journey. My grandparents, Marilyn and Richard, whose dedication and determination in their own fields set an example I will always aspire to follow. I would also like to thank the new additions to my family, the full Roberts-Pierel clan, for listening, laughing, and making me one of their own.

Finally, I have the **j**oy of acknowl**e**dging my fiancé, Justin, the person without whom, I am fair**l**y certain, this thesis would never have been started or finished. I **l**ook forward to another 8.2 decades of many successes (some fa**i**lures), but mostly a great deal of t**e**amwork. Last, but certainly not least, thanks to Amelia, Neil, and Tycho for your affection, attention, and admiration, it is much appreciated.

ABSTRACT

This study presents the first comparison of Landsat 8 OLI and Sentinel-2A MSI imagery in identifying soil salinity using soil physiochemical, spectral, statistical, and image analysis techniques. By the end of the century, intermediate sea level rise scenarios project approximately 1.3 meters (4.2 feet) of sea level rise along the coast of the southeastern United States. One of the most vulnerable areas is Hyde County, North Carolina, where 440 square miles of agricultural lands are being salinized, endangering 4,200 people and 40 million dollars of property. To determine the best multispectral sensor to map the extent of salinization, this study compared Landsat 8 OLI and Sentinel-2's identification of electrical conductivity (EC). The EC of field samples were correlated with handheld spectrometer spectra resampled into multispectral sensor bands. Using an iterative ordinary least squares regression, it was found that EC was sensitive to Landsat 8 OLI bands 2 and 4 and Sentinel-2A bands 2 and 6. Respectively, the R^2 and RSME of 0.04-0.54 and 0.90-1.90 for the OLI, and 0.04-0.69 and 0.73-2.83 for Sentinel-2, suggests that the increased spatial resolution of Sentinel-2 provides a more precise measurement of salinity location. Image analysis using band math estimates that salt crusts make up approximately 1.4% (Sentinel-2) to 2.57% (OLI) of bare soil indicating that surrounding land is saline though not currently identifiable through multispectral analysis. As sea levels rise, accurately monitoring soil salinization will be critical to protecting coastal agricultural lands. Sentinel-2's superior spatial and temporal resolution make it a superior sensor for salinity tracking.

PREFACE

Like many ideas, this research came out of a fortuitous meeting between members of the USDA Southeast Regional Climate Hub and myself at the Carolinas Climate Resilience Conference in the second week of my master’s degree. Little did I know that after many phone calls, emails, and discussions, I would be knee deep in salty mud in the beautiful Blacklands of North Carolina.

The longer I spent there taking soil samples and talking with locals, the more I realized that my thesis questions were just the tip of the iceberg. Thus, as such things are wont to do, my thesis is just the beginning of the complex web that connects local farmers to federal agencies, the atmosphere to the ocean and the ocean to the land, and the food producers to the food consumers. I cannot say at this moment where the story will end; however, I can assure you it will be a salty situation.

TABLE OF CONTENTS

LIST OF TABLES

LIST OF FIGURES

CHAPTER 1

INTRODUCTION

Coastal plains are some of the most vulnerable areas in the world to climate change, especially through the impacts of sea level rise. An inter-agency report published by the National Oceanic and Atmospheric Administration (NOAA) projects global mean sea level (GMSL) rise to be between 0.3 meters and 2.5 meters with the intermediate scenario at 1 m rise by 2100 (Sweet et al., 2017). The coast of North Carolina is projected to rise faster than the GMSL, reaching 1.3 m of rise by 2100 (Sweet et al., 2017). Increased storm surge and tide levels are already causing soil salinization in coastal counties.

Salinization can negatively impact crops. Increased salinity restricts water availability to plant roots similar to drought conditions (Brady & Weil, 2010; NRCS, 1998), decreases the germination rate for plants that directly results in yield loss (Ayers & Westcot, 1994; Brady & Weil, 2010; Hossain, 2010). Common commodity crops in coastal North Carolina are corn, soybeans, wheat, and cotton. Each crop experiences a yield declines at varying levels of EC (Table 1.1). Already, farmers are seeing impacts on the more sensitive crops if they are not carefully planted away from salinized areas. Ultimately, salinization can cost farmers hundreds of dollars per acre or even make land unusable for cultivation (Munns, Gilliham, Munns, & Gilliham, 2015). If nothing is done to mitigate soil salinization, increased coastal flooding will render the land unusable by the end of the century.

Measurement of salinity is critical for land management and mitigation. Electrical conductivity (EC), is a measurement of salt content in soil using a water solution or soil probe denoted as deciSiemens per metre (dS/m) (Brady & Weil, 2010). Saline soils generally have an EC greater than 4 dS/m. Even slightly salt-affected soils can impact plant growth depending on irrigation routines (Ghosh, Kumar, & Saha, 2012; Rhoades, 1982). Therefore, soil salinization tracking is critical to protecting coastal agricultural land. Farmers and agricultural extension agents believe that they lack state and federal support to respond to salinization because the extent of soil salinity is not well known (B.H.&E.C, personal communication, December 5, 2017). However, traditional methods of field surveying and sample analysing are not adequate to frequently cover large tracts of land (Li et al., 2015).

Table 1.1 Impact of salinity levels on crop yield potential (Ayers & Westcot, 1994)

	Crop Tolerance of Salinity (dS/m) and Yield Potential Impacts				
Crop	No impact on yield	10% yield loss	25% yield loss	50% yield loss	No crop growth
Corn (*Zea mays*)	<1.7	2.5	3.8	5.9	>10.0
Onion (*Allium cepa*)	<1.2	2.0	3.1	5.0	>8.9
Potato (Solanum tuberosum)	<1.7	2.5	3.8	5.9	>10.0
Cotton (*Gossypium hirsutum*)	<7.7	9.6	13	17	>27.0
Wheat (*Triticum aestivum*)	<6.0	7.4	9.5	13	>20.0
Soybean (*Glycine max*)	<5.0	5.5	6.3	7.5	>10.0

Satellite remote sensing offers the potential to cover a large spatial extent and provide regular measurements (Adam, Mutanga, & Rugege, 2009). Metternicht and Zinck (1997) and Metternicht (2003) used Landsat TM to detect salt-affected soils. Dwivedi and Sreenivas (1998) performed stepwise regression on MODIS bands to map salt-affected soils in the Indo-Gangetic alluvial plains. Accuracies of multispectral analysis, however, are limited primarily by large pixel size and broad bandwidths.

To address these limitations, studies have used hyperspectral data to study soil salinity (Ghosh et al., 2012; Li et al., 2015). Ghosh et al. (2012) integrated NASA's EO-1 Hyperion sensor and the Linear Mixture Model while Li et al. (2015) utilized the Chinese sensor HJ-1A to derive the Normal Soil Salt Content Response Index and the Soil Adjusted Vegetation Index. EO-1 was decommissioned in 2017 restricting its use to historical analysis (USGS, 2017). Additionally, current hyperspectral sensors (AVIRIS, Hyperion, CHRIS) do not have global coverage or high temporal resolution due to narrow swath widths, pointable platforms, or airplane-based missions (NASA, 2018; ESA, 2018; USGS, 2017). In lack of hyperspectral imagery, some studies integrated hyperspectral field spectra and physio-chemical measures with multispectral and very high resolution (VHR) data. Bai et al. (2016) Integrated in-situ measurements, similar to Li et al. (2015), though maintained the use of multispectral sensors for spatial and temporal coverage. Using stepwise regression, the study modelled the physio-chemical components of the soil using collected spectra and physio-chemical samples and Landsat OLI to identify soil alkalinity and salinity in the Songnen Plain of Northeast China. Bannari et al. (2008) built two indices for EO-1 ALI, a multispectral sensor, using spectra integration and in-situ measurements. Muller and Niekerk (2016) implemented analysis using WorldView-2 aggregated at a variety of resolutions to determine the effects of spatial resolution on salinity accuracy. The study concluded that VHR sensors were not necessary and potential candidates for future work were Sentinel-2 and SPOT6.

Each of these studies identified future pathways and limitations for soil salinity identification, highlighting the potential of hyperspectral sensors while also suggesting the use of higher resolution multispectral sensors. Due to the current limitations in hyperspectral data, timely soil salt detection must use multispectral data.

By combining the methodology of Bai et al. (2016) and higher spatial resolution from Sentinel-2 suggested by Muller and Niekerek (2016), this study presents the first comparison of Landsat OLI and Sentinel-2 for soil salt detection. The aim of this study is to compare the potential of mapping soil salinization using Landsat 8 OLI and Sentinel-2 following the methodology used in Bai et al. (2016). Correlations between the in-situ EC measurements and resampled multispectral bands were conducted. Using iterative ordinary least squares statistical modelling, the statistically significant models with the highest R^2_{Adj} and lowest collinearity were selected to map salinity in the study area.

CHAPTER 2

MATERIALS AND METHODS

2.1 Study Area

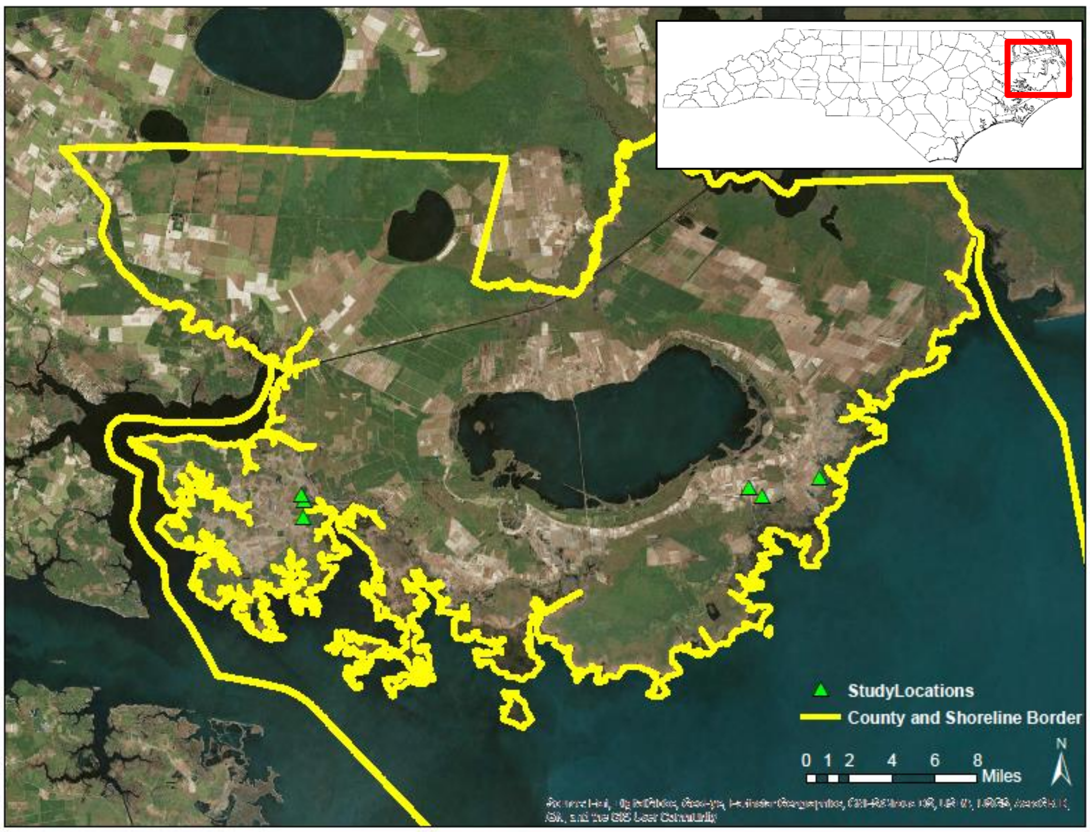

Figure 2.1 Hyde County, NC with the six soil sampling sites, each containing a 90 meter transect, represented as green triangles. The county extends into the Pamlico Sound to the island chain called the Outer Banks, this study only classified the continental portion of the county. Imagery from ESRI ArcGIS and Digital Globe.

Approximately 75 percent of land in Hyde County is below 1.3 meters of elevation (NOAA Office for Coastal Management, 2017). The highest elevation is in the west of the county along Alligator Lake at 4.4 meters of elevation (NRCS, 2001). In Hyde County, North Carolina, a 1.3 meter rise jeopardizes approximately 4,200 people, 440 square miles, and 40 million dollars in property including thousands of acres of agricultural land (Climate Central, 2016). According to the United States Department of Agriculture (USDA) 2012 Census of Agriculture there were 158 farms on the peninsula and total market value of agricultural products sold was $133 million (NASS, 2012).

The county was cleared and drained for cultivation in the 19th century using gravity-fed drainage ditches (McMullan Jr., Rich Jr., Landino, & Barnes, 2016). Rain-fed fields channel excess water into drainage ditches often only 24 inches wide. These ditches then cut along roads, through wetlands, and around fields before terminating at larger drainage canals or natural tributaries. Eventually, the water from the agricultural fields drains into the Pamlico Sound and the Atlantic Ocean following the gradient in elevation from land to sea. As sea level rises and the gradient shrinks, drainage ditches become tidal and, if not prevented, saltwater flows onto agricultural land during high tide and storm events (Manda, Giuliano, & Allen, 2014). Impacts of saltwater intrusion from ditches are observed through evidence of increased plant stress, salt crusts on soils, and agricultural abandonment (B.H., August 7, 2017; Moorhead & Brinson, 1995; Poulter et al., 2009).

Hyde County is located on the east coast of North Carolina covering an area of 613 mi^2. The county receives between 50 and 60 inches of rain annually with air temperatures between 50 and 75 degrees Fahrenheit. Approximately 70% of Hyde County is at or below 1.3 meters of elevation. According to a 2001 soil survey of the county, soils with a mineral surface layer or highly organic surface layer are most suitable for farming. Both soil groups have poor drainage capacity, requiring artificial drainage (NRCS, 2001). Agriculture accounts for almost 30% of the land and, together with forestry, fishing, and hunting approximately 19% of direct employment in the county (Data USA, 2016; NASS, 2012). The main crops grown are corn, cotton, soybeans, and wheat with some specialty vegetable cultivation.

2.2. Datasets and Pre-processing

2.2.1 Soil samples

Sample sites were selected based on a priori knowledge of salt damage and permission from landowners. Six fields were selected in total and a transect method was applied to collect soil samples along the salinity gradient away from drainage ditches (Figure 2.1). The transects were approximately 90 meters in length with samples taken every three meters on two dates for a total of 106 samples. The GPS locations of all sample points were recorded. Collection days were September 16, 2017 and December 05, 2017. 54 samples were collected in September and 52 samples were collected in December. These dates were chosen due to their proximity to Landsat 8 OLI overpass times. The dry fall in Hyde County made salt crusts apparent on soil surface and decreasing interference from soil moisture (SM); however, the December date had higher soil moisture due to recent precipitation. Soil moisture was directly measured using the FieldScout TDR 150 in December and a the North American Land Data Assimilation System (NLDAS-2) Noah Lands Surface Model was used as a proxy for surface soil moisture (0-10 cm) in September (Xia et al., 2012). Due to vegetation interference, several transects were shortened during collection.

Measurements of EC and spectra were conducted in the field. A JAZ Ocean optics handheld spectrometer was held 1 meter above the sample point to collect reflectance spectra. The spectrometer has 2,048 bands from 191.117 nm to 889.222 nm (VIS) (OceanOptics, 2018). A FieldScout TDR 150 was used to measure EC, SM, and temperature in-situ. The 4.5 inch probes were inserted into the soil and measurements were recorded (Spectrum Technologies, 2017). Five samples were submitted for validation testing at the North Carolina State University Agricultural Cooperative Extension Service lab.

The JAZ spectrometer data was pre-processed using Python programming. Due to high noises in the shortwave infrared (SWIR), the spectra were limited to 400-760 nm (VIS-NIR). Reflectance (r) was calculated from the raw count using the equation:

$$r = \frac{s-d}{k-d} * 100 \tag{1}$$

where s is the raw count data and k and d are the reference and dark spectra, respectively, taken while calibrating the spectrometer in-situ.

2.2.2. Satellite Imagery and Pre-processing

Satellite images from Landsat 8 OLI and Sentinel-2 were used in this study. Sentinel-2 is a European Space Agency mission that includes two polar-orbiting satellites (Sentinel-2A and Sentinel-2B) allowing the return time to be decreased from 10 to 5 days at the equator and less in the mid-latitudes (ESA, 2017). A Sentinel-2A image was used in this study. Landsat OLI has a return time of 16 days (USGS, 2016). OLI has four bands within the VIS-NIR at 30 m spatial resolution and Sentinel-2A has six bands at 10-20 meter spatial resolution (ESA, 2017; USGS, 2016). The OLI image used in this study was taken September 16, 2017. The Sentinel-2 image was taken September 20, 2017. The OLI image was downloaded from USGS Data Clearinghouse (EarthExplorer). Using ENVI 5.4, the image was then radiometrically calibrated and converted to surface reflectance using the Fast Line-of-Sight Atmospheric Analysis of Spectral Hypercubes (FLAASH) module. The Sentinel-2 image was corrected and converted to reflectance using the European Space Agency Sentinel Application Platform (SNAP) Sen2Cor module (ESA, 2014).

Two masks were used to exclude the non-soil pixels in both images. First, the normalized difference vegetation index (NDVI) was used to identify vegetation and water pixels. As per previous studies, pixels with NDVI > 0.3 were considered vegetation and NDVI<0.05 were considered water (Bai et al. 2016). The ENVI module "Calculate Cloud Mask using Fmask" was then used to remove any clouds from the images. The final images contained only bare soil pixels.

2.3. Methodology

A Pearson's *r* correlation was conducted between the processed JAZ data and 100 soil EC measurements (Equation 2). Pearson's *r* measures the linear correlation between two variables though it can be affected by outliers and sample size (Pearson, 1895). This data is approximately normally distributed (skewness ±2) (Gravetter & Wallnau, 2014). The Pearson's *r* correlation is calculated as:

$$r = \frac{\sum XY - \frac{(\sum X)(\sum Y)}{n}}{\sqrt{(\sum X^2 - \frac{(\sum X)^2}{n})(\sum Y^2 - \frac{(\sum Y)^2}{n})}} \tag{2}$$

where X represents the reflectance value, Y represents the EC, and n is the total number of values in each dataset (n must be equal for X and Y). In addition, a continuum removal of the JAZ data was implemented by fitting a convex hull to the spectra to identify absorptions and emissions in the spectra to determine the viability of future hyperspectral satellite research. The processed, not continuum removed JAZ data was resampled to the broad multispectral bands using the Landsat OLI and Sentinel-2 spectral response functions (J. A. Barsi et al., 2011; J. Barsi et al., 2014; ESA, 2017) to better compare the two sensors. A Pearson's R correlation analysis was conducted between the resampled spectra and the field measured EC using 100 samples. Correlation coefficients indicate the strength and direction of relationships between variables. The statistical significance of the correlation was tested at the 0.05 significance level.

Then, an iterative ordinary least squares regression was used to develop two models for OLI and Sentinel-2 using the appropriate resampled data. The OLI model had four independent variables (Bands 1-4) and Sentinel-2 model had six independent variables (Bands 1-6). 67 samples were used for model development with 33 samples used for validation. The samples were selected randomly to avoid bias. Stepwise regressions have been used previously; however, it has been shown that the results lead to a higher chance of spurious statistical significance, parameter bias, and inconsistencies leading to non-replicable results (Thompson, 1995; Whittingham et al., 2006). Due to this possibility, two main statistical metrics were measured to evaluate model performance. To avoid collinearity from the related variables that can cause prediction errors, the variance inflation (VIF) was calculated (Equation 3). Finally, the Akaike's Information Criterion (AIC) was used to compare the resulting regression models and rank the models (Equation 4). To use AIC, the models must already satisfy the informative requirements of the other four statistics. A VIF>5 indicates high collinearity. Generally, the lowest model AIC score is best though models with a $\Delta_i < 2$ have essentially equivalent value in goodness of fit and models with a $\Delta_i > 10$ are poor enough to not be considered. There is some debate on the Δ_i between 2 and 10 and this study considered all models with a $\Delta_i < 6$ from the best AIC score (Burnham & Anderson, 2002; Symonds & Moussalli, 2010). VIF and AIC are calculated as:

$$VIF = \frac{1}{1-R^2} \tag{3}$$

$$AIC = n\left[\ln(\frac{RSS}{n})\right] + 2k \tag{4}$$

Three additional metrics were used in coordination with VIF and AIC. The coefficient of determination (R^2) is a measure of the goodness of fit between measured and predicted values (Equation 5). R^2_{Adj} adjusts for the over-fit of the model (Equation 6). The root mean square error (RMSE) is an estimate of error within the model (Equation 7). These statistics are calculated as:

$$R^2 = 1 - \frac{\sum_{i=1}^{n}(\gamma-\gamma')^2}{\sum_{i=1}^{n}(\gamma'-\bar{\gamma})^2} \tag{5}$$

$$R^2_{Adj} = 1 - \frac{n-1}{n-k-1}(1-R^2) \tag{6}$$

$$RMSE = \sqrt{\frac{\sum_{i=1}^{n}(\gamma-\gamma')^2}{n}} \tag{7}$$

where γ are the measured EC values, γ' are the predicted EC values, $\bar{\gamma}$ is the average of measured values, n is the number of samples (n=66), and k is the number of variables (k=4 (OLI), k=6 (Sentinel-2)). An iterative approach was used to developing the model due to the known constraints of stepwise regression models (Thompson, 1995). Each model was evaluated using the full validation dataset and datasets consisting of the individual days of observation. This was done to identify potential errors during sampling.

Finally, the regression models were applied to analyse Landsat OLI and Sentinel-2A scenes. Using the pre-processed imagery and the ENVI Band Math module, the EC was calculated for each bare soil pixel. The resulting values were then validated using 33 field samples and VHR imagery from Google Earth. The VHR imagery was visually interpreted to identify salt crusts based on a priori field observations. Landsat OLI and Sentinel-2 results were compared using statistical analysis, spectral sensitivity analysis, and accuracy assessments.

CHAPTER 3

RESULTS

3.1 Soil Sample Salinity Gradient

As hypothesized, a gradient of high to low salinity existed from the edges of the fields near the drainage ditches to towards the centres of the fields (Figure 3.1). This shows that the salinity is likely coming from overland saltwater inundation during high tides or storm events.

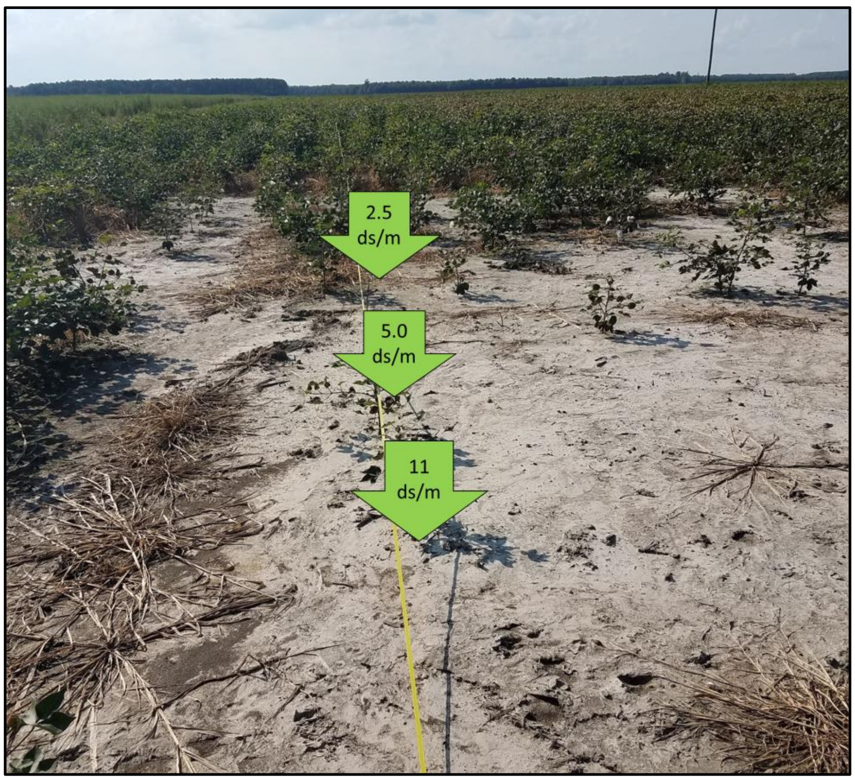

Figure 3.1 Example gradient of soil electrical conductivity levels away from drainage ditches

3.2 Spectral Properties of Soil Samples

EC measurements in the study area ranged from 11 dS/m to 0 dS/m. Metternicht and Zinck (1997) categorized below 4 dS/m as non-saline, between 4 dS/m and 8 dS/m as slightly saline, between 8 dS/m and 16 dS/m as moderately saline, and above 16 dS/m as strongly saline. However, even an EC of 4 dS/m can result in a crop yield loss of between 25 and 50 percent for corn, onions, and potatoes (Ayers & Westcot, 1994). Due to the impact of lower salinity on crops, the threshold of 4 dS/m was determined sufficient for identifying areas of critical salinity. Therefore, soil spectra in this study were examined based on two EC classes (above and below 4 dS/m) to demonstrate salinity-related spectral variation.

In Figure 3.2a, saline soils (above 4dS/m) have significantly higher spectral reflectance than non-saline soils (below 4 dS/m). Continuum removal was conducted to demonstrate the wavelengths of spectral absorption and emission that could correspond with salinity (Figure 3.2b). The wavelength ranges of highest reflectance are 403-412 nm, 420-453 nm, 566-588 nm, 596-608 nm, 719-736 nm, and 743-750 nm. Figure 3.3 shows the correlation coefficients between EC and soil reflectance, as a function of wavelength. Correlation coefficients were the highest between 400 and 500 nm with a decreasing trend toward the NIR. Starting at 688 nm a sharp increase in the p-value indicates a lack of statistical significance.

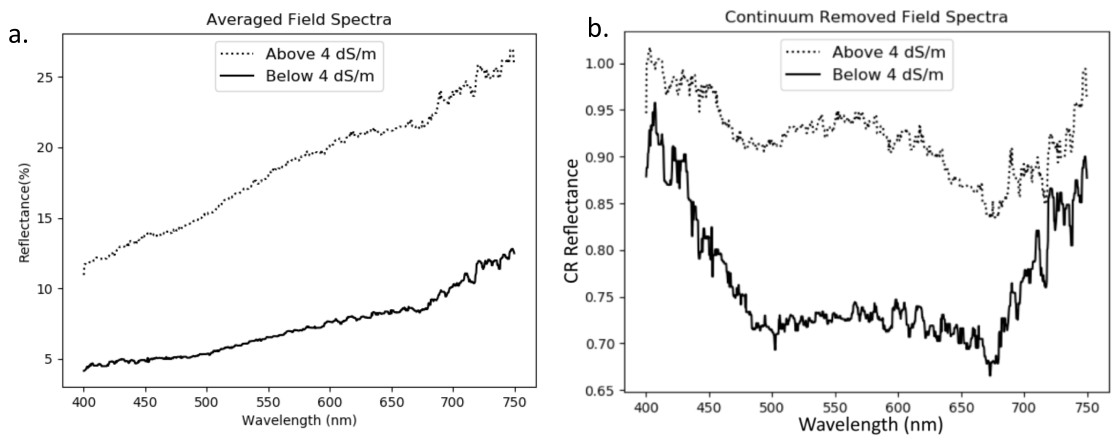

Figure 3.2 Calculated Reflectance of field spectra (a) averaged into above and below 4 dS/m categories (b) continuum removed.

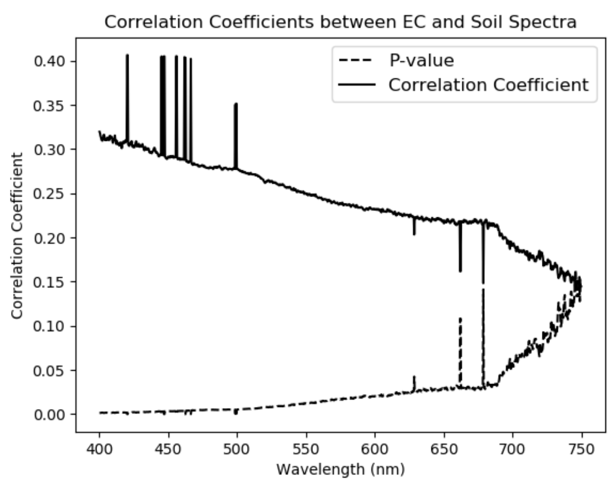

Figure 3.3 Correlation coefficient and P-value between EC and not continuum removed Soil Spectra

3.3. Resampled Spectrometer Analysis

The narrow spectral features identified by hyperspectral sensors are less easily detected by broad brand sensors. Tables 3.1 and 3.2 show the correlation coefficients between the satellite-like bands and EC for both sensors. The correlation coefficients stay fairly close to the hyperspectral coefficients for similar spectral ranges. The OLI-like bands have slightly higher correlation coefficients though Sentinel-like bands have consistently statistically significant results. Due to the high correlations between the bands, there is a high likelihood of collinearity between the bands as identified.

Table 3.1 Pearson r correlation coefficients among the OLI-like bands and EC.

Bands in nm	b1	b2	b3	b4	EC
b1 (434-451)	1				
b2 (452-512)	0.90*	1			
b3 (533-590)	0.73*	0.94*	1		
b4 (636-673)	0.68*	0.92*	0.98*	1	
EC	0.42	0.35*	0.25*	0.21*	1

*Significant at the 0.05 probability level

Table 3.2 Pearson r correlation coefficients for sample spectra averaged into Sentinel-2 bands

Bands in nm	b1	b2	b3	b4	b5	b6	EC
b1 (433-453)	1						
b2 (457.5-522.5)	0.98*	1					
b3 (542.5-577.5)	0.89*	0.95*	1				
b4 (650-680)	0.85*	0.93*	0.98*	1			
b5 (697.5-712.5)	0.82*	0.90*	0.98*	0.98*	1		
b6 (732.5-747.5)	0.78*	0.87*	0.95*	0.96*	0.99*	1	
EC	0.39*	0.35*	0.25*	0.21*	0.18*	0.14	1

*Significant at the 0.05 probability level

3.4. Regression Model

The resulting models were statistically significant with the lowest AIC, and no significant multicollinearity. In the Landsat OLI model, Bands 2 (452-512 nm) and 4 (636-673 nm) were sensitive to EC. In the Sentinel-2 model, Bands 2 (457.5-522.5) and 6 (732.5-747.5) were sensitive to EC. This suggests that the Blue and Red spectral ranges are the most sensitive to EC in both sensors. Equation 8 shows the Landsat OLI model with OLI Band 2 and 4. Equation 9 shows the Sentinel-2 model with Band 2 and 6.

$$EC_{OLI} = 2.0080 + 0.0698\boldsymbol{b2} - 0.0156\boldsymbol{b4} \quad (8)$$

$$EC_{Sentinel-2} = 2.1111 + 0.0559\boldsymbol{b2} - 0.0074\boldsymbol{b6} \quad (9)$$

The descriptive statistics of the models describe the performance of each regression model (Table 3.3). The R^2_{Adj} for the Landsat OLI model and Sentinel-2 model were lower for the December collection day than for the September collection day though both were statistically significant. The R^2_{Adj} for Landsat OLI on the first day was 0.33 and with all data 0.20. The R^2_{Adj} for the Sentinel-2 model was 0.412 on day one of sampling and 0.234 including both days of sampling. The RMSE of the Landsat OLI and Sentinel-2 models are 1.24 and 1.42, respectively. This indicates that they could both be used to predict EC though Sentinel-2 has slightly higher skill.

There are three potential factors that may explain these differences in model fitting between the two days. In September, the crops were at the end of the growing season but had mostly not been harvested while in December the crops were harvested and the land was tilled causing a change in soil texture and surface soil type. Soil moisture between September and December were approximately equivalent. However, the lab soil tests confirmed the EC measurements were accurate regardless of the change in soil moisture. The lab soil tests showed a clear relationship between field salinity measurements and lab salinity measurements (Figure 3.4). As EC is a function of soil moisture and salt concentration, the two variables are highly correlated (Pearson r of .78) even small variations could have affected the in-situ measurements. Additionally, temperature is a potential factor as temperature varied between 17 °C and 28 °C in September and 6 °C and 19 °C in December.

Table 3.3 Model statistics for both sampling days, separated and combined, the bolded categories are statistically significant.

Day	Sensor	R^2	R^2_{Adj}	RMSE	VIF	AIC
September	**Landsat OLI**	**0.54**	**0.51**	**0.90**	**2.17**	**172.5**
	Sentinel-2	**0.69**	**0.669**	**0.73**	**3.23**	**165.4**
December	Landsat OLI	0.04	-0.02	1.90	1.04	229.6
	Sentinel-2	0.04	-0.02	2.83	1.04	228.2
Both Days	**Landsat OLI**	**0.31**	**0.24**	**1.15**	**1.45**	**333.80**
	Sentinel-2	**0.32**	**0.27**	**1.13**	**1.47**	**331.90**

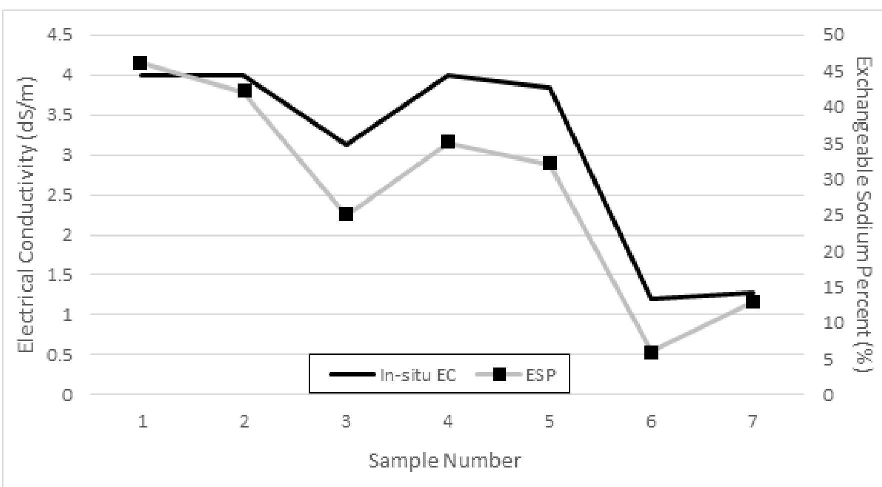

Figure 3.4 Soil test results adapted from NCDA&CS Agronomic Division showing Exchangeable Sodium Percent (ESP) and In-situ Electrical Conductivity (EC)

3.5. Comparison of salinity mapping

The OLI and Sentinel-2A models were applied to their respective images. Only the above 4 dS/m soils were extracted for the final salinity distribution analysis. Using the Sentinel-2A and Landsat OLI images, salinized soils cover approximately 1.8% (529 acres) (Sentinel-2A) to 2.5% (4210 acres) (Landsat OLI) of the bare soil in Hyde County, most of which is farmland. The area was calculated as the percentage of bare soil (extract through the masking process) classified as saline by the models. Image analysis identified only the highest salinity pixels, although in-situ soil measurements reveal that surrounding pixels were also saline. This is likely due to the high spectral reflectance of salt crusts versus lower saline soils or soils that have recently been disturbed through tilling or harvesting.

Salt-affected soils are clustered together and around water bodies, inlets, and low elevations indicating the impact of elevation and saltwater flooding on increased soil salinity. Location (Figure 3.5) and concentration (Figure 3.6) maps were created to visually display the comparison between the Landsat OLI and Sentinel 2 images. The concentration map was created using hot spot analysis based on polygon area density. Both sensors highlight three areas with high densities of saline soils, the northwest corner of the county, southwest corner, and east coast (Figure 3.6). Manmade structures that reflect brightly such as light pavement and metal roofs are improperly classified by both OLI and Sentinel-2.

As seen in Figures 3.5 and 3.6, OLI classifies more soil area as saline (>4 dS/m) than Sentinel-2. This can be explained by the larger pixel size and the overestimation due to lower model accuracy. In comparing Sentinel-2 and Landsat OLI, it is clear that OLI overestimates the spatial extent of visible high salinity soils on a pixel per pixel basis.

Figure 3.7 shows an example using Digital Globe imagery from ArcGIS of a high salinity soil location and the difference in identification between OLI and Sentinel-2. However, both sensors underestimate the full scale of soil salinization due to difficulties identifying low salinity (<4 dS/m) soils. Sentinel-2's higher spatial resolution enabled the identification of narrow salt crusts through fields while the salt signal was lost or overestimated with Landsat OLI.

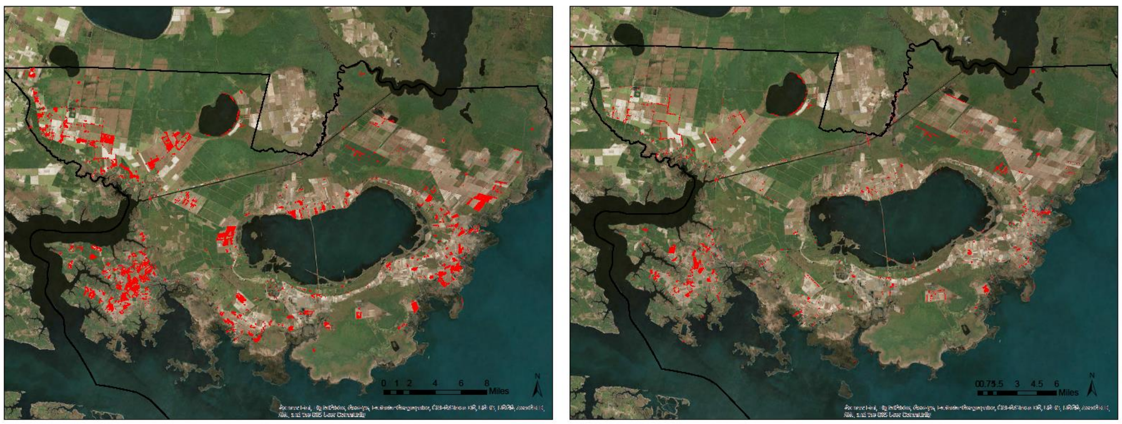

Figure 3.5 Distribution of soil salinity in Hyde County, NC from Landsat OLI (a) and Sentinel-2 (b), red pixels are identified as saline

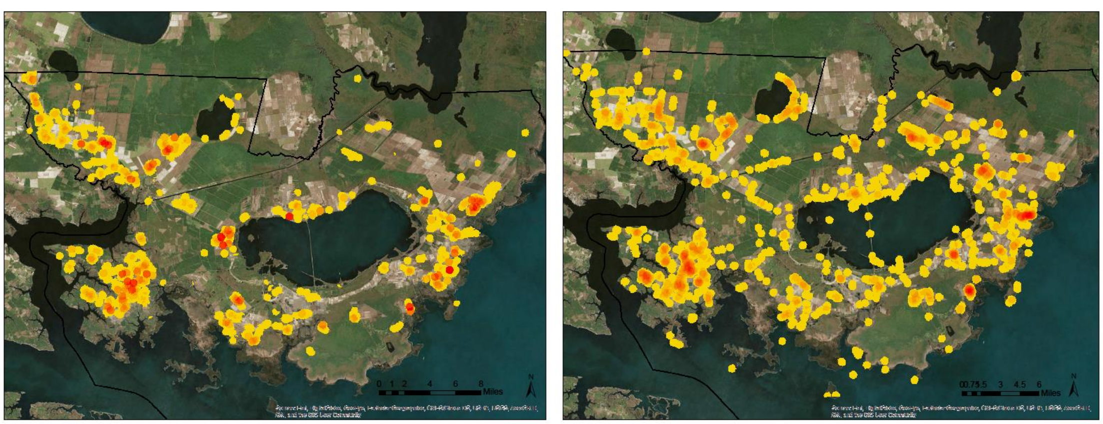

Figure 3.6 Concentrations of soil salinity pixels in Hyde County, NC from Landsat OLI (left) and Sentinel-2 (right)

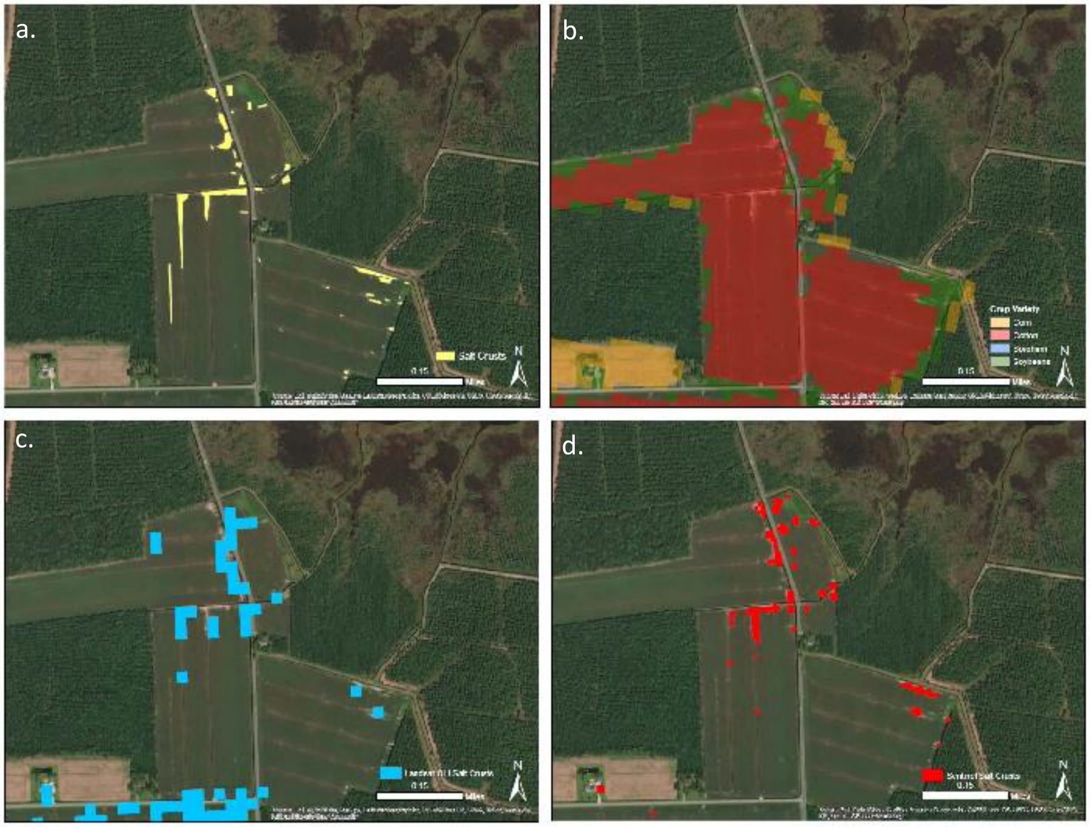

Figure 3.7 Example of salt crust locations, identified through visual interpretation (a) in comparison with the USDA NASS Crop Data Layer (b), Landsat OLI modelled salt crusts (c), and Sentinel-2 modelled salt crusts (d).

Sensitivity of Landsat OLI and Sentinel-2 to salt vary due to spectral resolution and band location (Figure 3.8). Sentinel-2 is able to better capture the upward trajectory of the JAZ spectrometer spectra (insitu) in the red to NIR bands. Landsat OLI is more closely related to the in-situ spectra in the shorter wavelengths. At band 3 (approximately 560 nm), all three spectra are in near agreement. This result shows that multispectral data, while lacking in the resolution of hyperspectral data, is still able to capture with some sensitivity the field spectra of saline soils.

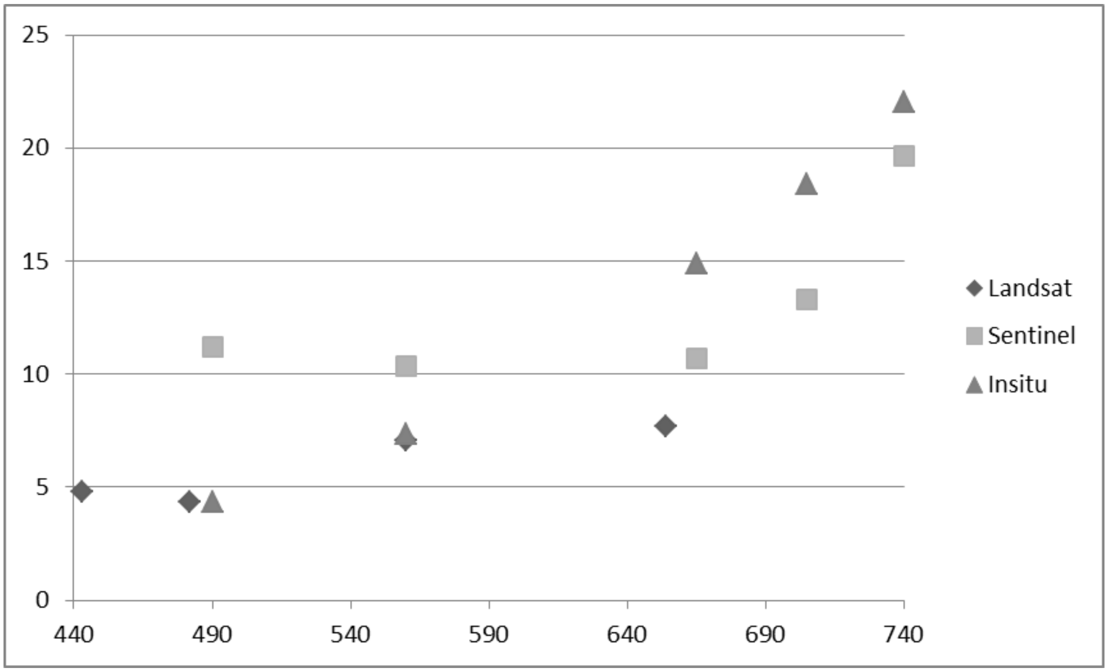

Figure 3.8 Spectral Sensitivity for Landsat OLI, Sentinel-2, and JAZ spectrometer

CHAPTER 4

DISCUSSION

4.1. Use of multispectral data for salinity tracking

To date, Sentinel-2 has not been used for the identification of salinity though previous work has indicated that it might be superior to other broad band imagery (Muller & Van Niekerk, 2016). In this comparative study, correlation coefficients remained nearly the same between the broadband spectra of Landsat OLI and Sentinel-2 with correlated with EC. Statistically significant relationships existed for both OLI and Sentinel-2 aggregated bands when correlated with EC, indicating both OLI and Sentinel-2 can predict the location of soil salinity.

Using linear regression models, OLI bands 2 (452 nm-512 nm) and 4 (636 nm-673 nm) and Sentinel-2 bands 2 (457.5 nm-522.5 nm) and 6 (732.5 nm – 747.5 nm) were selected to estimate soil EC. Both models were statistically significant and showed low collinearity. The models have relatively flat slopes, enabling them to capture the values around 4 dS/m but overestimating the low EC values and underestimating the high EC values.

The variation in R^2_{Adj} between sampling days suggest that there may be environmental factors impacting EC and spectral reflectance. Soil texture changes and temperature variations due to measuring before and after the harvest season are potential explanations. The dew point and humidity varied between the two days which may have impacted spectral readings. The dew point and average relative humidity in nearby Dare County were 67°F and 90 for September and 59°F and 92 for December (Weather Underground, 2017). Soil moisture did not vary extensively between days but varied between the sampling sites. As the spectra and EC were measured in-situ, and not in a lab, noise and anomalous measurements likely contributed to the limited fit of the models. Previous studies processed field data in a lab resulting in EC and spectral measurements under ideal, controlled circumstances (Bai et al., 2016; Ghosh et al., 2012; Li et al., 2015; G. Metternicht & Zinck, 1997). Due to the less controllable environment when taking measurements in-situ, higher variation in sample spectra and EC measurements may be explained. This study is in agreement with previous studies in the identification of bands useful for modelling high soil salinity (Bai et al., 2016; Li et al., 2015).

Overall, Sentinel-2 is shown to be the more useful dataset for identifying salinity change in coastal landscapes. The R^2_{Adj} and RMSE of the models indicate that Sentinel-2 has slightly better skill than Landsat OLI at predicting EC. Sentinel-2's 10 meter spatial resolution and 2-3 day return time also offers superior spatial and temporal resolution to Landsat OLI's 30 meter spatial resolution and 16 day return time. When taking into account in-situ measurements showing that salinity impacted land continued beyond the land mapped using the models, the estimate of land affected rises significantly, however, without hyperspectral data, it is difficult to definitively quantify.

4.2. Agricultural Implications

Based on the results of this study, salinity can be mapped in agricultural land in Hyde County, NC. Sentinel-2 and Landsat OLI have similar limitations to their spectral resolution when classifying saline soils though Sentinel-2 has a slightly higher resolution. Only the highest salinity soils are mapped using this multispectral methodology approach, so the values of 1.4%-2.5% of the land are likely underestimations in terms of total affected land. In addition, land that is experiencing salinity problems but is vegetated with halophyte plants or is not saline enough to significantly decrease crop yields is not included in this mapping approach, although in-situ soil measurements indicate these areas exist. The higher spatial resolution of Sentinel-2 decreases the number of mixed pixels likely lending to a higher accuracy in classification. Increased spatial resolution and classification accuracy aids in tracking and addressing soil salinization in agricultural fields. As sea levels rise, land will either need to be protected or practices will need to be adapted to the changes though barriers exist for both of these options.

4.3. Opportunities for Future Research

This study tests the feasibility of advancing the use of multispectral imagery from two satellite sensors for salinity identification. Currently, Sentinel-2 provides superior spatial, spectral, and temporal resolutions to Landsat OLI leading to improved salinity classification. Results for both classification models may be improved by conducting lab-based EC and spectral sampling to reduce environmental noise, taking a greater number of samples to reduce potential bias, taking samples during the drier months of the year to increase salt signatures, and sampling either before or after harvesting to decrease texture interference.

To address the spectral limitations of broadband data such as that from Landsat OLI and Sentinel-2, previous studies have employed hyperspectral data to improve soil salinity classification (Ghosh et al., 2012; Li et al., 2015). The hyperspectral JAZ spectrometer measurements show more sensitivity to soil salinity than the broadband sensors, particularly after continuum removal. This indicates that future work should involve analysis using hyperspectral imagery. Currently, the ESA CHRIS sensor and Chinese HJ-1 satellite constellation provide hyperspectral data. The HJ-1 sensor was effectively used by Li et al. (2015) though has been shown to have some data limitations. The Italian Space Agency PRISMA mission is scheduled to launch in December 2018 and will contain a hyperspectral sensor (OHB Italia, 2018). Additionally, the NASA Hyspiri satellite is estimated to be launched after 2022 (California Institute of Technology, n.d.). For historical analysis, Hyperion data from pre-2017 can be used. or Although there are limitations, Sentinel-2 offers the potential for high spatial and temporal resolution salinization tracking that is both economical and computationally efficient.

CHAPTER 5

CONCLUSION

This study conducted soil spectra and EC measurements to compare the skill of Landsat OLI and Sentinel-2 in mapping soil salinity extent. Statistically significant correlations exist between EC and both Landsat 8 OLI and Sentinel-2 bands. The Landsat 8 OLI and Sentinel-2 estimation models had R2Adj of 0.33 and 0.41, respectively. In-situ soil measurements instead of lab measurements may account for the relatively lower R2Adj than previous studies. High salinity soils, that often appeared as white salt crusts, (>4 dS/m) covered approximately 1.4%-2.57% of the county, although in situ measurement of soil salinity indicated that this is likely an underestimation of the total affected area. As sea levels rise, soil salinization will increase, and continuous tracking of salinity change is necessary to respond to the threat.

Due to the higher spatial resolution, predictive ability, and return time, Sentinel-2 offers superior opportunities for identification of salinity than Landsat OLI However, analysis of hyperspectral handheld spectrometer measurements suggest that hyperspectral sensors may have increased predictive ability in identification of soil salinity.

REFERENCES

Adam, E., Mutanga, O., & Rugege, D. (2009). Multispectral and hyperspectral remote sensing for identification and mapping of wetland vegetation: a review. *Wetlands Ecol Management*. Retrieved from https://www.researchgate.net/profile/Onisimo_Mutanga/publication/225456909_Multispectral_and_hyperspectral_remote_sensing_for_identification_and_mapping_of_wetland_vegetation_A_review/links/09e4150e6b7617a58a000000/Multispectral-and-hyperspectral-remote-s

Ayers, R., & Westcot, D. (1994). *Water quality for agriculture*. Retrieved from http://www.fao.org/docrep/003/T0234E/T0234E03.htm#ch2.4.3

Bai, L., Wang, C., Zang, S., Zhang, Y., Hao, Q., & Wu, Y. (2016). Remote sensing of soil alkalinity and salinity in the Wuyu'er-Shuangyang river basin, Northeast China. *Remote Sensing*, *8*(2). https://doi.org/10.3390/rs8020163

Bannari, A., Guedon, A. M., El-Harti, A., Cherkaoui, F., & El-Ghmari, A. (2008). Characterization of slightly and moderately saline and sodic soils in irrigated agriculture land using simulated data of advanced land imaging (EO-1) sensor. *Communications in Soil Science and Plant Analysis*, *39*(19–20), 2795–2811. https://doi.org/10.1080/00103620802432717

Barsi, J. A., Markham, B. L., & Pedelty, J. A. (2011). The operational land imager: spectral response and spectral uniformity. In J. J. Butler, X. Xiong, & X. Gu (Eds.) (p. 81530G). https://doi.org/10.1117/12.895438

Barsi, J., Lee, K., Kvaran, G., Markham, B., & Pedelty, J. (2014). The Spectral Response of the Landsat-8 Operational Land Imager. *Remote Sensing*, *6*(10), 10232–10251. https://doi.org/10.3390/rs61010232

Brady, N. C., & Weil, R. R. (2010). *Elements of the Nature and Properites of Soils* (Third Edit). Upper Saddle River: Prentice Hall.

Burnham, K. P., & Anderson, D. R. (2002). *Model Selection and Multimodel Inference: A Practical Information-Theoretic Approach* (2nd ed.). New York: Springer-Verlag.

California Institute of Technology. (n.d.). Welcome to HyspIRI Mission Study Website — Hyperspectral Infrared Imager. Retrieved January 22, 2017, from https://hyspiri.jpl.nasa.gov/

California institute of Technology, & NASA. (2018). AVIRIS. Retrieved May 17, 2018, from https://aviris.jpl.nasa.gov/aviris/index.html

Data USA. (2016). Hyde County, NC. Retrieved May 17, 2018, from https://datausa.io/profile/geo/hyde-county-nc/

Dwivedi, R. S., & Sreenivas, K. (1998). Image transforms as a tool for the study of soil salinity and alkalinity dynamics. *International Journal of Remote Sensing*, *19*(4), 605–619. https://doi.org/10.1080/014311698215883

ESA. (2014). Sentinel-2 Toolbox Tutorials | STEP. Retrieved April 22, 2018, from http://step.esa.int/main/doc/tutorials/sentinel-2-toolbox-tutorials/

ESA. (2017). Sentinel-2 Spectral Response Functions (S2-SRF) - Sentinel-2 MSI Document Library - User Guides - Sentinel Online. Retrieved April 22, 2018, from https://earth.esa.int/web/sentinel/user-guides/sentinel-2-msi/document-library/-/asset_publisher/Wk0TKajiISaR/content/sentinel-2a-spectral-responses

European Space Agency. (2018). CHRIS. Retrieved May 17, 2018, from https://earth.esa.int/web/guest/missions/esa-operational-eo-missions/proba/instruments/chris

Ghosh, G., Kumar, S., & Saha, S. K. (2012). Hyperspectral Satellite Data in Mapping Salt-Affected Soils Using Linear Spectral Unmixing Analysis. *Journal of the Indian Society of Remote Sensing*, *40*(1), 129–136. https://doi.org/10.1007/s12524-011-0143-x

Gravetter, F., & Wallnau, L. (2014). *Essentials of Statistics for the Behavioral Sciences* (8th ed.). Belmont, CA: Wadsworth.

Li, J., Pu, L., Zhu, M., Dai, X., Xu, Y., Chen, X., … Zhang, R. (2015). Monitoring soil salt content using HJ-1A hyperspectral data: A case study of coastal areas in Rudong County, Eastern China. *Chinese Geographical Science*, *25*(2), 213–223. https://doi.org/10.1007/s11769-014-0693-2

Manda, A. K., Giuliano, A. S., & Allen, T. R. (2014). Influence of artificial channels on the source and extent of saline water intrusion in the wind tide dominated wetlands of the southern Albemarle estuarine system (USA). *Environmental Earth Sciences*, *71*(10), 4409–4419. https://doi.org/10.1007/s12665-013-2834-9

McMullan Jr., P. S., Rich Jr., C., Landino, J., & Barnes, S. (2016). *North Carolina's Blacklands Treasure*. (P. W. Carroll, Ed.). Nags Head, NC: Pamlico & Albemarle Publishing.

Metternicht, G. ., & Zinck, J. . (2003). Remote sensing of soil salinity: potentials and constraints. *Remote Sensing of Environment*, *85*(1), 1–20. https://doi.org/10.1016/S0034-4257(02)00188-8

Metternicht, G., & Zinck, J. A. (1997). Spatial discrimination of salt- and sodium-affected soil surfaces. *International Journal of Remote Sensing*, *18*(12), 2571–2586. https://doi.org/10.1080/014311697217486

Moorhead, K., & Brinson, M. (1995). Response of Wetlands to Rising Sea Level in the Lower Coastal Plain of North Carolina. *Ecological Society of America*, *5*(1), 261–271. Retrieved from http://www.jstor.org.pallas2.tcl.sc.edu/stable/pdf/1942068.pdf

Muller, S. J., & Van Niekerk, A. (2016). Identification of WorldView-2 spectral and spatial factors in detecting salt accumulation in cultivated fields. https://doi.org/10.1016/j.geoderma.2016.02.028

NASS. (2012). *Hyde County 2012 Agricultural Census*. Retrieved from https://www.agcensus.usda.gov/Publications/2012/Online_Resources/County_Profiles/North_Carolina/cp37095.pdf

NRCS. (2001). Soil Survey of Hyde County, North Carolina. *Spring*, 1–202.

OceanOptics. (2018). Jaz Series - Ocean Optics. Retrieved April 22, 2018, from https://oceanoptics.com/product-category/jaz-series/

OHB Italia. (2018). Home. Retrieved June 1, 2018, from http://prisma-i.it/index.php/en/

Pearson, K. (1895). Notes on regression and inheritance in the case of two parents. *Proceedings of the Royal Society of London*, *58*, 240–242. Retrieved from https://books.google.com/books?id=60aL0zlT-90C&pg=PA240#v=onepage&q&f=false

Poulter, B., Feldman, R. L., Brinson, M. M., Horton, B. P., Orbach, M. K., Pearsall, S. H., … Whitehead, J. C. (2009). Sea-level rise research and dialogue in North Carolina: Creating windows for policy change. *Ocean and Coastal Management*, *52*(3–4), 147–153. https://doi.org/10.1016/j.ocecoaman.2008.09.010

Rhoades, J. D. (1982). Soluble Salts. *Agronomy Monograph*, *9*, 167–178.

Spectrum Technologies, I. (2017). TDR 150 Soil Moisture Meter with Case | Spectrum Technologies. Retrieved April 22, 2018, from https://www.specmeters.com/soil-and-water/tdr-150-soil-moisture-meter-with-case/

Symonds, M. R. E., & Moussalli, A. (2010). A brief guide to model selection, multimodel inference and model averaging in behavioural ecology using Akaike's information criterion. *Behavioral Ecology Sociobiology*, *65*, 13–21. https://doi.org/10.1007/s00265-010-1037-6

Thompson, B. (1995). Stepwise regression and stepwise discriminant analysis need not apply here: A guidelines editorial. *Educational and Psychological Measurement*, *55*(4). Retrieved from http://journals.sagepub.com/doi/pdf/10.1177/0013164495055004001

USGS. (2016). Landsat 8 | Landsat Missions. Retrieved March 11, 2017, from https://landsat.usgs.gov/landsat-8

USGS. (2017). Earth Observing 1 (EO-1). Retrieved May 17, 2018, from https://eo1.usgs.gov/

Weather Underground. (2017). Weather History & Data Archive. Retrieved July 4, 2018, from https://www.wunderground.com/history/

Whittingham, M. J., Stephens, P. A., Bradbury, R. B., & Freckleton, R. P. (2006). Why do we still use stepwise modelling in ecology and behaviour? *Journal of Animal Ecology*, *75*(5), 1182–1189. https://doi.org/10.1111/j.1365-2656.2006.01141.x

Xia, Y., Mitchell, K., Ek, M., Sheffield, J., Cosgrove, B., Wood, E., … Mocko, D.

(2012). Continental-scale water and energy flux analysis and validation for the North American Land Data Assimilation System project phase 2 (NLDAS-2): 1. Intercomparison and application of model products. *Journal of Geophysical Research: Atmospheres*, *117*(D3), n/a-n/a. https://doi.org/10.1029/2011JD016048